^{129}Xe Nuclear Shielding and Diffusion in the A and C* Phases of a Chiral Smectogen

Mario Cifelli,[†] Jani Saunavaara,[‡] Jukka Jokisaari,*[,‡] and Carlo A. Veracini*[,†]

Department of Chemistry and Industrial Chemistry, University of Pisa, Italy, and NMR Research Group, Department of Physical Sciences, University of Oulu, Finland

Received: January 15, 2004

The ^{129}Xe NMR shielding and diffusion of xenon dissolved in the chiral liquid-crystal 1-methylheptyl 4′-(4-*n*-decyloxybenzoyloxy)biphenyl-4-carboxylate (10B1M7) were studied over the temperature range covering the isotropic (I), smectic A (SmA), and ferroelectric, ferrielectric, and antiferroelectric smectic C*(SmC*) phases. The ^{129}Xe shielding reveals clearly the I−SmA and SmA−SmC*(ferroelectric) phase transitions. The SmC* sub-phase transitions can also be detected by smaller but distinguishable shifts of the shielding accompanied by line width changes. A theoretical model developed earlier is applied to the shielding data, confirming a negative anisotropic contribution to the shielding as the SmA phase forms and allowing the evaluation of the tilt angle in the SmC*. Diffusion experiments were mostly performed in the direction parallel to the layer normal, i.e., along the external magnetic field, $D_{\parallel}$, in the smectic phases but a few experiments were carried out in the in-plane direction, i.e., perpendicular to the external magnetic field, $D_{\perp}$, as well. These experiments indicate large anisotropy, $D_{\perp}/D_{\parallel}$, of the ^{129}Xe diffusion tensor that increases as the temperature decreases. Application of the Arrhenius equation to the temperature-dependence of $D_{\parallel}$ reveals different activation energies for each studied phase. This can be correlated to changes in the smectic layer structure that occur between the different smectic phases.

Introduction

There has recently been much effort devoted to elucidating the structure and polar properties of ferroelectric (FLC) and antiferroelectric (AFLC) phases assembled by chiral smectogens in case of a high enantiomeric excess.[1] The interest in these mesophases stems from their polar properties connected to spontaneous or field induced broken symmetries[1] that can provide a high impact in technological applications, in particular in the LCD manufacturing.[2] Continuous experimental work and several theoretical models have been put forward in attempting to explain the role of chirality, the microscopic nature of molecular organization, and molecular reasons for the phase transitions and synclinic to anticlinic layer arrangements.

NMR of noble gases (helium, neon, krypton and xenon) dissolved in liquid crystals is a very applicable means to derive information on the physical properties of liquid crystals. A particularly suitable noble gas isotope is ^{129}Xe because its shielding is extremely sensitive to even very subtle changes in the environment. On the other hand, NMR of the quadrupolar isotopes, ^{21}Ne, ^{83}Kr, and ^{131}Xe, may be utilized in deriving complementary information as they interact with the electric field gradient created by the liquid-crystal molecules.[3,4]

Other ^{129}Xe NMR spectroscopic methods, although somewhat more tedious ones as compared to chemical shift measurements, yield valuable information on liquid crystals are spin−lattice, T_1, and spin−spin relaxation, T_2, experiments and diffusion measurements at variable temperatures. The former have been applied, for example, to study the mixture of 6OCB (4-cyano-4′-*n*-hexyloxybiphenyl) and 8OCB (4-cyano-4′-*n*-octyloxybiphenyl) on one hand and the mixture of 7CB (4-*n*-heptyl-4′-cyanobiphenyl), 8OCB, and 5CT (4-*n*-pentyl-4′-cyanoterphenyl) on the other hand, both displaying a re-entrant nematic phase.[5] In these particular cases, the ^{129}Xe chemical shift does not indicate any significant change at the nematic−SmA transition, contrary to other findings,[6−8] whereas clear change is detected when approaching the re-entrant nematic phase from the smectic A phase. When plotting $\ln(T_1)$ and $\ln(T_2)$ as a function of inverse temperature the slope of the resulting straight lines within the various phases is observed to change significantly, indicating varying activation energies.[5]

The ^{129}Xe diffusion experiments in the isotropic, nematic, smectic A, and smectic C* phases of a commercial ferroelectric liquid crystal, FELIX-R&D (from Hoechst), revealed the diffusion tensor to be very anisotropic and the anisotropy, $D_{\perp}/D_{\parallel}$, increases toward the C* phase. The large anisotropy is interpreted to arise from the layer structure of smectic phases; xenon diffuses rather along the layer surface where density is smaller than through the denser core region. The shielding data, furthermore, indicate that xenon atoms are redistributed during the formation of the layer structure so that part of the atoms is expelled from the dense core region to the less dense interlayer space.[7,8]

The structural properties of the present liquid crystal, 1-methylheptyl 4′-(4-*n*-decyloxybenzoyloxy)biphenyl-4-carboxylate (10B1M7), were earlier studied with applying ^{2}H NMR to partially deuterated species, the deuterons being either in the phenyl ring or in the biphenyl moiety.[9] In this paper, the orientational order parameter, the tilt angle in the SmC* phase, and the molecular structure of the aromatic cores of the

* To whom correspondence should be addressed. Prof. Jukka Jokisaari: Department of Physical Sciences, P.O. Box 3000, University of Oulu, Finland 90014. Phone: +358-8-5531308 or +358-40-5956146. Fax: +358-8-5531287. E-mail: Jukka.Jokisaari@oulu.fi. Prof. Carlo A. Veracini: Dipartimento di Chimica e Chimica Industriale, Università di Pisa, Via Risorgimento 35, Pisa, Italy 56126. Phone: +39-0502219266. Fax: +39-0502219260. E-mail: verax@dcci.unipi.it.

[†] University of Pisa.

[‡] University of Oulu.

10.1021/jp049788o CCC: $27.50
Published on Web 04/13/2004

mesogenic molecule were investigated. In the context of this study, a sharp decrease of the deuterium NMR line width as the SmC*(ferroelectric)−SmC*(ferrielectric) phase transition occurs was pointed out,[9] in contrast to no relevant changes in the orientational order linked quadrupolar coupling and in the rotational dynamics investigated by means of ^{2}H T_1 Zeeman and quadrupolar studies.[10] The reasons of this phenomenon are still under investigation.[11]

Experimental Section

All of the experiments were performed on a Bruker Avance DRX500 spectrometer equipped with a BVT2000 variable temperature unit. A 5-mm BBI probe with integrated Z-gradient coils was used for both shielding and diffusion experiments, whereas the experiments with a 10-mm sample and some $D_\perp$ diffusion measurements at high temperatures were carried out with a 10-mm BB probe. The 10-mm sample contained 0,76 g of a mixture of 10B1M7 and partially deuterated 10B1M7−$2d_2$ LC and ca. 3 atm of ^{129}Xe enriched (80%) xenon gas, whereas the 5-mm sample contained 0.50 g of 10B1M7 LC and ca. 2 atm of ^{129}Xe enriched xenon gas. Temperature was calibrated with a sample of ethylene glycol (80%) in DMSO.

The ^{129}Xe diffusion constant in the direction of the external magnetic field, $D_{||}$, was determined over the temperature range covering the isotropic, smectic A, and smectic C* phases of 10B1M7 by applying the pulsed gradient method (PGSE) introduced by Stejskal and Tanner.[12] Some double spin−echo (DSE) experiments were also carried out in order to check whether convection effects are present.[8] Since no convection was found, the PGSE method was mostly applied in order to attain a good S/N ratio in a reasonable time. In the experiments with the pulsed gradients the following parameters were used: (PGSE) $\delta = 3.8-25.2$ ms, $\Delta = 45.6-171.1$ ms and (DSE) $\delta = 2.95-25.7$ ms, $\Delta = 43.35-66.05$ ms. Ramped gradient pulses with five equal increments (decrements) were used with constant gradient duration of 40 or 50 ms and ramp step delay of 50 μs. A few experiments were carried out in the perpendicular direction to the external magnetic field in order to gain information about the possible anisotropy of the diffusion tensor. The CTPG (constant time, pulse and gradient) has been used, creating a steady gradient perpendicular to the main field direction with the aid of the shim coils.[13] In the experiment, the following parameters were used: $G = 0.92-2.4$ mT m^{-1} and $\tau_1 + \tau_2 = 0.4-1.2$ s.

All of the measurements were started by warming the sample to a high temperature in which it was clearly in the isotropic phase. Then the temperature was lowered with steps of 1−2 K to cover the phases of 10B1M7. A major problem with measurements was the limited temperature range of the 5-mm BBI gradient probe; the I−SmA phase transition temperature of the sample is ca. 397 K, and consequently, the I phase is outside the probe's temperature range. Thus, the experiments in the isotropic phase were performed as quickly as possible, and therefore, equilibration time may have been too short at the highest temperatures, leading to resonance line broadening. Furthermore, the reorientation of the LC director seems to be very slow; it appeared that especially at the SmC* phases the ^{129}Xe signal is at its best only several hours after the temperature change.

Results and Discussion

Application of a Theoretical Model to the Experimental ^{129}Xe NMR Shielding. The chemical shielding was determined from the maximum of the single line of the xenon spectra and is plotted as a function of temperature in Figure 1. The uncertainty of the shielding values was estimated from the line width, *S*/*N* ratio, and digital resolution. In the isotropic phase (I), lines appeared broad because of relatively large temperature gradients due to working at temperatures outside the probe head range and consequent too short equilibrium times. The error in shielding in the I and SmA phases is 0.05 and 0.02 ppm, respectively. As the SmC* forms, lines start to become broader, the shape deforms, and the uncertainty increases to about 0.1 ppm.

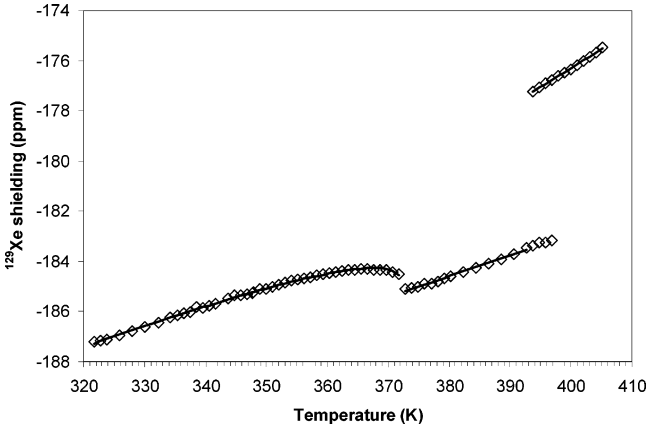

Figure 1. Experimental ^{129}Xe shielding constant (relative to low-pressure xenon gas) at variable temperatures for xenon in the 10B1M7 liquid crystal. The solid line is the result of the least-squares fits as described in the text.

The ^{129}Xe chemical shift behavior in the liquid-crystalline environment can be modeled with the function[7,8,14]

$$\sigma(T) - \sigma_0 = \rho(T)\Big\{\sigma_d'[1 - \epsilon(T - T_0)](1 + 2c\gamma_1^2(T)) + \frac{2}{3}P_2(\cos\theta)\Delta\sigma_d'[1 - \Delta\epsilon(T - T_0)][S(T) + 2c\sigma_1(T)\gamma_1(T)]\Big\} \quad (1)$$

where the temperature-dependence of the shielding constant and shielding anisotropy is assumed to be linear and is described by the coefficients ϵ and $\Delta\epsilon$, respectively.[14] In eq 1, σ_0 is the shielding constant of the reference (low-pressure xenon gas in the present case), T_0 is the reference temperature (chosen to be the I−SmA phase transition temperature 396.7 K), and σ_d' and $\Delta\sigma_d'$ are temperature-independent isotropic shielding constant and the anisotropy of the shielding tensor (in ppm/g^{-1}cm^3), respectively. The anisotropic part in the shielding arises from the deviation of the xenon electron cloud from spherical symmetry because of the anisotropic surrounding. The coefficient *c* measures the deviation of the xenon distribution from uniform distribution, and $S(T)$, $\sigma_1(T)$, and $\gamma_1(T)$ are orientational order parameters: $S(T)$ is the normal second rank orientational order parameter, $\sigma_1(T)$ is the mixed translational-orientational order parameter, and $\gamma_1(T)$ is the translational order parameter. $P_2(\cos\theta)$ is the second-order Legendre polynomial with θ being the angle between the liquid-crystal director and the external magnetic field.

The density of liquids and liquid crystals is generally linearly dependent upon temperature within conventional temperature ranges and can be represented as

$$\rho(T) = \rho_0[1 - \alpha(T - T_0)] \quad (2)$$

where ρ_0 is density at the reference temperature T_0 and α is the

thermal expansion coefficient. Strictly speaking, eq 2 may not be valid over the whole isotopic−smectic range in liquid crystals but only within each phase. Namely, the density may change discontinuously at phase transitions; at the isotropic−nematic transition, the change may be 2−3% but much smaller, however, at other transitions.[15] Introducing eq 2 to eq 1 leads to

$$\sigma(T) - \sigma_0 = [1 - \alpha(T - T_0)]\Big\{\sigma_d[1 - \epsilon(T - T_0)]\,(1 + 2c\gamma_1^2(T)) + \frac{2}{3}P_2(\cos\theta)\Delta\sigma_d[1 - \Delta\epsilon(T - T_0)]\,[S(T) + 2c\sigma_1(T)\gamma_1(T)]\Big\} \quad (3)$$

where $\sigma_d = \rho_0\sigma_d'$ and $\Delta\sigma_d = \rho_0\Delta\sigma_d'$ (both in ppm) are independent of temperature.

The possible density jumps at the phase transitions of the 10B1M7 LC are not known to us. Therefore, they cannot be taken into account in the following analysis of shielding data. On the other hand, as stated above, they are generally small at the SmA−SmC* transitions and consequently do not introduce large errors, for example, when deriving the tilt angle in the SmC* phase as discussed below. Although density jumps were omitted, the thermal expansion coefficient α was assumed different in the isotropic and smectic phases and was kept as a free parameter in the fits. Another effect that we have neglected is the bulk susceptibility correction to the shielding data. In principle, this effect should be considered because the experimental shielding values are taken relative to an external (low-pressure xenon) gas reference. The susceptibility correction, σ_b, for a long cylindrical liquid-crystalline sample is[14]

$$\sigma_b = -\frac{1}{3}\Big[\chi + \frac{2}{3}\Delta\chi S(T)\Big]\frac{\rho(T)}{M} \quad (4)$$

where χ is the isotropic average of the diamagnetic volume susceptibility tensor and $\Delta\chi$ is the anisotropy of the tensor and M molar mass. Again assuming that the density changes continuously over the whole studied temperature range, it can be concluded that (when using some typical values for χ and $\Delta\chi$) eq 4 leads to practically constant correction to the experimental shielding. Consequently, the exclusion of the correction does not affect significantly the results derived below, particularly when keeping in mind the experimental error in the shielding data which is relatively large at low temperatures where the resonance lines become broad, as stated above.

Isotropic Phase. In the isotropic phase of a liquid crystal, all of the orientational order parameters vanish, i.e., $S(T) = \sigma_1(T) = \gamma_1(T) = 0$. Consequently, When the first-order approximation (the term second order in T is omitted) is applied, the ^{129}Xe shielding can be written in a simple form

$$\sigma(T) - \sigma_0 = [1 - (\alpha + \epsilon)(T - T_0)]\,\sigma_d \quad (5)$$

The least-squares fitting procedure with keeping $T_0 = 396.7$ K fixed, while adjusting $(\alpha + \epsilon)$ and σ_d, leads to $(\alpha + \epsilon) = 8.44 \times 10^{-4}$ K^{-1} and $\sigma_d = -176.795$ ppm. The $(\alpha + \epsilon)$ value is close to the typical thermal expansion coefficient values of liquid crystals.[15] Thus, we may conclude that the variation of the isotropic shielding constant is, in this particular case, practically exclusively due to the variation of LC density with temperature and $\epsilon \approx 0$.

Smectic A Phase. In the smectic A phase, the liquid-crystal director orients along the external magnetic field, and consequently, $P_2(\cos\theta) = 1$. Utilizing the observation made in the isotropic phase, i.e., $(\alpha + \epsilon) \approx \alpha$, and assuming on this basis that also $(\alpha + \Delta\epsilon) \approx \alpha$, eq 3 reduces as

$$\sigma(T) - \sigma_0 = [1 - \alpha(T - T_0)]\Big\{\sigma_d[1 + 2c\gamma_1^2(T)] + \frac{2}{3}\Delta\sigma_d[S(T) + 2c\sigma_1(T)\gamma_1(T)]\Big\} \quad (6)$$

TABLE 1: Values of the Parameters Kept Fixed or Varied in Fitting the Experimental ^{129}Xe Shielding Data to Theoretical Models as Explained in the Text

parameter	value		
	Isotropic Phase		
α	8.44×10^{-4} K^{-1}		
σ_d[a]	−176.795 ppm		
	Smectic Phases		
α	7.37×10^{-4} K^{-1}		
$\Delta\sigma_d$	−19.259 ppm		
c	−0.0325		
$S(T)$[b]	$y_s = 0.9995$	$z_s = 0.0927$	
$\sigma_1(T)$[b]	$y_\sigma = 0.9995$	$z_\sigma = 0.2173$	
$\tau_1(T)$[b]	$x = 0.1562$	$y_\gamma = 0.9995$	$z_\gamma = 0.2198$
θ_0	33.38°		
β	0.142		

[a] Assumed to be the same in all the LC phases. [b] Kept fixed in the least-squares fit.

The orientational order parameters are modeled with the functions[7,16,17]

$$S(T) = \left(1 - y_S\frac{T}{T_0}\right)^{z_s} \quad (7)$$

$$\sigma_1(T) = \left(1 - y_\sigma\frac{T}{T_0}\right)^{z_\sigma} \quad (8)$$

and

$$\gamma_1(T) = \left(1 + x\frac{T}{T_0}\right)\left(1 - y_\gamma\frac{T}{T_0}\right)^{z_\gamma} \quad (9)$$

which appear to describe well the temperature-dependence of these parameters.[7] Now the following parameters should be adjusted (σ_d was kept fixed at the value derived in the isotropic phase): α, $\Delta\sigma_d$, c, y_s, z_s, y_σ, z_σ, x, y_γ, and z_γ. Thus, there are 10 adjustable parameters which is absolutely too many for this particular problem. Therefore, only α, $\Delta\sigma_d$, and c were adjusted while the other parameters were fixed to the values shown in Table 1 together with the values of the adjusted parameters. The parameter values are physically quite reasonable and reproduce, together with the orientational order parameters given above, the shielding behavior as shown in Figure 1.

The thermal expansion coefficient $\alpha = 7.37 \times 10^{-4}$ K^{-1} of the smectic phase is somewhat smaller than that of the isotropic phase in accordance with an earlier observation.[7] The anisotropy of the shielding tensor, $\Delta\sigma_d$, appears to be −19.26 ppm which is close to the value reported for xenon in the SmA phase of the NCB84 (1-butyl-c-4-(4′-octylbiphenyl-4-yl)-r-1-cyclohexan-carbonitrile) liquid crystal.[7] All of the experiments till now concerning the ^{129}Xe shielding anisotropy of xenon in liquid crystals have revealed negative shielding anisotropy, and as seen, this study is not an exception. This leads to the situation that, in the isotropic−smectic (or nematic if it exists) phase transition, the experimental shielding decreases in cases where the LC director orients along the external magnetic field as seen also in Figure 1. The parameter c is found to be −0.032, meaning that the positional distribution function of xenon in 10B1M7 deviates ca. 3.2% from the uniform distribution. This further

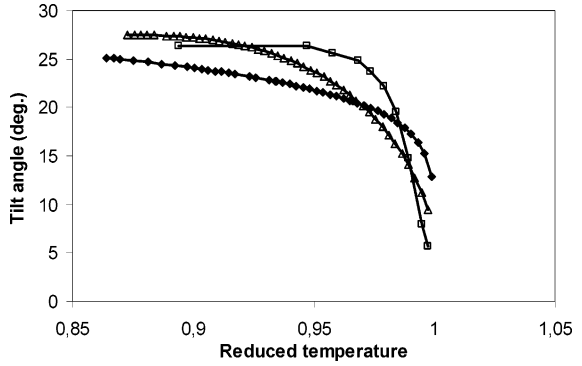

Figure 2. Tilt angle of the director in the SmC* phases of 10B1M7 as a function of reduced temperature, T/T_{AC*}, from the present ^{129}Xe shielding values (◆) and from the ^{2}H NMR experiments (△).[9] The points (□) were estimated from Figure 17 of ref 22 and are from optical measurements.

means that xenon atoms rather occupy the interlayer space than the layer space of a smectic phase.

Smectic C* Phases. The SmC* phase is characterized by the appearance of a temperature-dependent tilt between the phase director and the smectic layer normal. This is defined by the tilt angle θ, and for a smectic phase formed of chiral molecules, it produces a decrease of symmetry in the phase that leads to a spontaneous polarization vector.[18,19] This spontaneous polarization is minimized in the phase by a helical structure that winds along the layer normal producing no net macroscopic polarization in the phase orthogonal to the layer normal.[1] The nonchiral, nonpolar smectic C phase aligns with the director parallel to the static $\mathbf{B_0}$ field,[20] hence minimizing the effect of the magnetic field. Conversely the SmC* preferentially aligns the layers normally to the static $\mathbf{B_0}$ field, compromising the interaction with the field and the chiral helical tilted structure.[1] This behavior has been already investigated by means of ^{2}H NMR, and the tilt angle was derived comparing the quadrupolar coupling in the SmA and SmC* phases.[9] The quadrupolar coupling was considered proportional to the tilt angle

$$\Delta\nu_Q \propto P_2(\cos\theta) \tag{10}$$

where $\theta = 0$ in the SmA phase and nonzero in the Sm C* phase. In the case that no abrupt changes in orientational order parameters occur at the phase transition, the tilt angle was derived from the ratio between the SmA phase quadrupolar coupling extrapolated to the SmC* temperature range and the actual measured value in the tilted phase.[9]

In the present case, the term $P_2(\cos\theta)$ in eq 3, and consequently the tilt angle θ, can be determined as a function of temperature under the approximation that molecular order and density change continuously at the SmA−SmC* phase transition. In practice, this means that the ^{129}Xe shielding in the SmA phase (extrapolated to the region of the SmC* phase) and the experimental ^{129}Xe shielding in the SmC* phase are assumed to differ exclusively because of the tilt of the LC director. The temperature-dependence of the tilt angle can be modeled using a power law[21]

$$\theta(T) = \theta_0\left(1 - \frac{T}{T_{AC*}}\right)^{\beta} \tag{11}$$

where T_{AC*} is the SmA−SmC* phase transition temperature and β and θ_0 are phenomenological parameters. Nonlinear least-squares fitting leads to $T_{AC*} = 372$ K, $\theta_0 = 33.38°$, and $\beta = 0.142$. Figure 2 displays the temperature dependence of the tilt angle and comparison with the ones determined by ^{2}H NMR[9] and by optical measurements.[22] Agreement of the present result with the earlier findings is good, particularly when keeping in mind the approximations made. This is the first time that ^{129}Xe NMR is exploited in deriving the tilt angle in a SmC* phase.

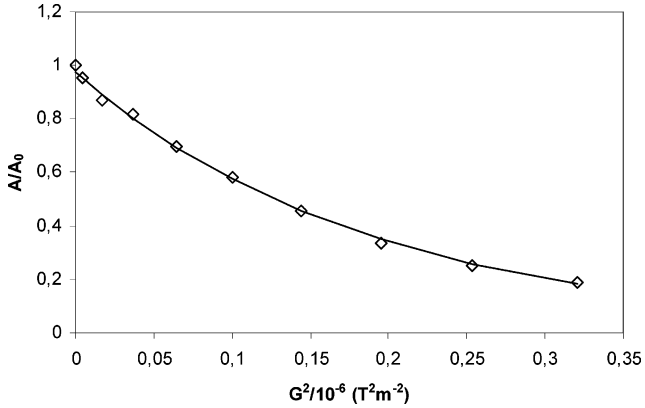

Figure 3. Relative ^{129}Xe echo amplitude as a function of the square of the pulsed magnetic field gradient at $T = 388$ K where the 10B1M7 liquid crystal appears in the smectic A phase. The points (◇) are from experiments and the solid line from least-squares fit to function (12).

Xenon Diffusion Measurements. The ^{129}Xe diffusion coefficient along the external magnetic field, $D_{||}$, was determined from the echo amplitude attenuation as a function of the strength of the magnetic field gradient pulse. In Figure 3, an example of the echo amplitude decay is shown for ^{129}Xe in the SmA phase at T = 388 K. As can be seen, the decay of the relative echo amplitude A/A_0 is well reproduced by the known equation[23]

$$\frac{A}{A_0} = \exp\left[-(\gamma G)^2\left(\delta^2\left(\Delta - \frac{3}{\delta}\right) + \frac{d^3}{30} - \frac{\delta\, d^2}{6}\right)D_{||}\right] \tag{12}$$

where A_0 is a normalization factor, Δ is the diffusion time, d is the increment (decrement) time of the gradient, and $\delta = d + h$ with h being the duration of the constant gradient G.[8]

The diffusion coefficient in the perpendicular direction, $D_{\perp}$, was determined at a few temperatures from the CTPG echo amplitude attenuation as a function of the τ_1 and τ_2 echo times from eq 13

$$\frac{A}{A_0} = \exp\left[-\frac{2}{3}(\gamma G)^2(\tau_1{}^3 + \tau_2{}^3)D_{\perp}\right] \tag{13}$$

The diffusion coefficients $D_{||}$ and $D_{\perp}$ measured in the isotropic and liquid-crystalline phases of 10B1M7 are reported in a logarithmic scale as a function of the inverse of temperature in Figure 4. The uncertainty in $D_{||}$'s has been estimated to be less than 7%, whereas in $D_{\perp}$'s, it is ca. 10%.

Looking at Figure 4, some interesting features can be brought forth: (a) As the SmA phase forms, a large diffusion anisotropy $D_{\perp}/D_{||}$ occurs and it increases as the temperature decreases, for example, from ca. 3.3 to ca. 9.5 when moving from 386 to 359 K. (b) In the smectic phases, the diffusion coefficient $D_{||}$ decreases monotonically as the temperature decreases by about 2 orders of magnitude from the SmA to the SmC*(antiferroelectric) phase, whereas $D_{\perp}$ decreases more slowly. (c) No sharp changes can be detected in the diffusion coefficient $D_{||}$ at the phase transitions, apart from the relevant change when passing from the nonordered isotropic phase to the smectic A phase. (d) The temperature-dependence of the diffusion coefficient in each phase can be well fitted with the Arrhenius equation$D(T) = D_0 \exp(-E_a/RT)$.

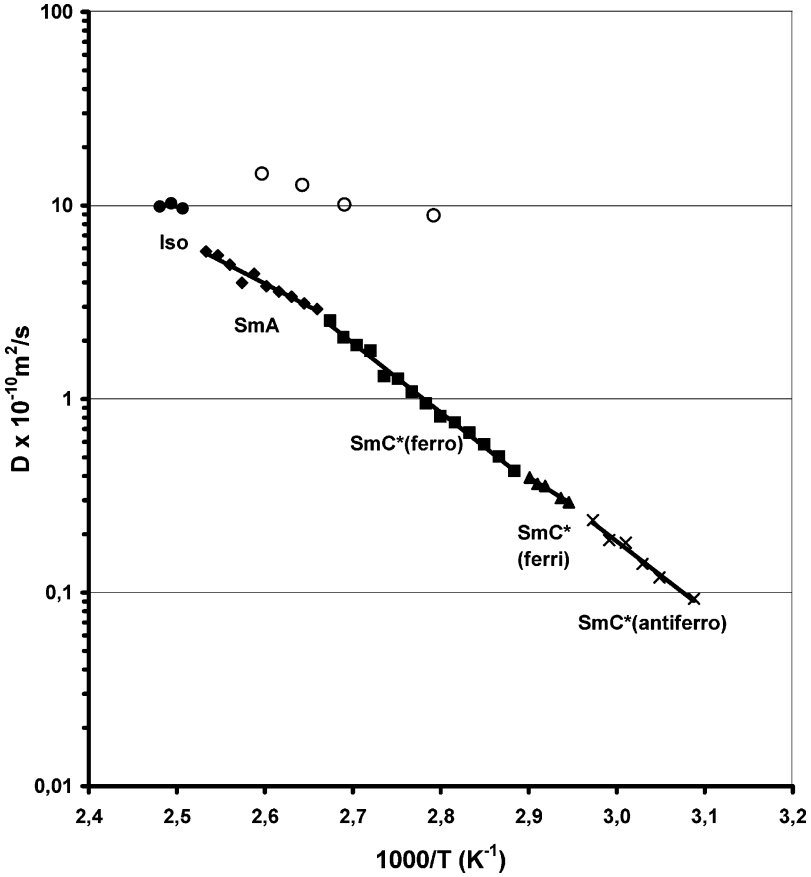

Figure 4. Diffusion coefficients of xenon in the isotropic and smectic phases of 10B1M7 as a function of inverse temperature. $D_\perp$ was measured only at four temperatures and is indicated by (○). The other points indicate the experimental $D_\parallel$ values, whereas the solid lines represent Arrhenius fits in the various phases.

Diffusion anisotropy $D_\perp/D_\parallel > 1$ is typical for globular probes in smectic phases and has already been noted, i.e., for methane diffusing in the SmA phase of 8CB (4-cyano-4′-octylbiphenyl),[24] PDT (perdeuterated tempone) in the smectic cyano-biphenyl mixture S2,[25] and xenon in a commercial chiral smectogen FELIX-R&D.[8] It can be rationalized as follows. In the isotropic phase, the xenon atoms diffuse within stochastically distributed rigid aromatic cores and flexible aliphatic chains that form a nonordered environment. As the SmA phase is assembled, the layer structure creates dense aromatic cores regions, intercalated with less ordered and more flexible aliphatic chains. In this situation, the small xenon atoms are expelled from the aromatic cores and more favorably dwell in the aliphatic regions. Consequently, the xenon atoms experience a high potential barrier when diffusing across the smectic layers, but they can diffuse quite easily in the flexible aliphatic chains, explaining the $D_\perp/D_\parallel > 1$ relation. Going a step further, it is hence reasonable to think that the diffusion process described by $D_\perp$ represents diffusion across a loose aliphatic only region that hinders diffusion less than the isotropic phase.

The temperature-dependence of the translational diffusion can be utilized to determine some information about the ordering of the smectic phases.[26] A model for the temperature dependence of translational diffusion in liquid-crystal phases has been proposed by Moscicki and co-workers in terms of the free-volume theory.[25] In this approach, a diffusing particle spends most of the time in a cage delimited by its neighbors and diffusion takes place only after density fluctuations can enlarge the cavity enough for the particle to move through. Hence, diffusion happens as a consequence of a redistribution of the free volume in the liquid. In terms of the model, the cage expansion depends on the phase free energy, the local compressibility, and the ratio between the probe length l and the interlayer distance, t and Moscicki and co-workers wrote down expressions for the excess activation energies (in respect to the isotropic one) for the parallel and perpendicular diffusional processes.[25] In particular, for a small globular probe ($l \ll t$)

TABLE 2: ^{129}Xe Diffusion Activation Energies for the Various Liquid-Crystalline Phases of 10B1M7 as Derived from the Temperature Behavior of $D_\parallel$

phase	activation energy (kJ/mol)
smectic A	46.8 ± 1.4
smectic C*(ferroelectrid)	67.6 ± 2.0
smectic C*(ferrielectric)	53.4 ± 2.5
smectic C*(antiferroelectric)	67.1 ± 2.0

$$\Delta E_\parallel \cong k\mu\Lambda\gamma_1 \tag{14}$$

where k is the compressibility, μ and Λ are xenon related potential parameters, and γ_1 is the translational order parameter of the smectic phase. In this view, the activation energy for the diffusion along the external magnetic field in the smectic phase can be expressed as

$$E_{all} = E_{iso} + \Delta E_\parallel \tag{15}$$

where E_{iso} is activation energy in the isotropic phase. In the present case, the activation energies have been determined by Arrhenius fittings in the smectic phases. Best fitting activation energies have been obtained with an error of only a few percent, and the values are reported in Table 2. The fitting curves are

reported in Figure 4 with the experimental values of the diffusion coefficients.

Unfortunately, at the present stage, no reliable comparison can be made between the isotropic activation energy and the one determined in the smectic A phase, due to the high-temperature limitation of the applied probe head in measuring diffusion in the isotropic phase. Regarding the activation energies in the LC phases it can be noticed that $E_{a||} > E_{a\perp}$ which stems from the same reasons as previously discussed regarding the diffusion tensor anisotropy. Analogous results have been reported in earlier investigations for globular probes in thermotropic liquid-crystals phases [24,25] and in particular for xenon in the chiral smectogen FELIX-R&D.[8] In that case, however, the large uncertainty in the diffusion constants perpendicular to the external magnetic field did not allow us to actually define the activation energy, and a behavior similar to the isotropic phase has been implied.[8]

As can be noted from Table 2, the activation energy in the SmC* phase is over 40% larger than in the SmA phase. When considering the xenon parameters μ and Λ constant through the phase, a change in the smectic translational order parameter γ_1 or phase compressibility k can be invoked. The appearance of the tilt of the phase director relative to the smectic planes can be related to an increase in compressibility, and moreover, the tilted structure can pose extra hindrance to the diffusion along the external magnetic field even in the case of no relevant change in the smectic positional ordering, consequently increasing the activation energy for the xenon. The other interesting feature is the sharp decrease (ca. 21%) of the activation energy from the SmC*(ferroelectric) to the SmC*(ferrielectric) phase and the subsequent increase (ca. 25%) in the SmC*(antiferroelectric) phase. These activation energy changes of xenon can be considered as a probe of changes in the SmC* sub-phases.

Previous investigations of phase textures of 10B1M7 by means of polarized optical microscopy pointed out relevant changes in the helical structure of the SmC* phases that was related to different degrees of molecular dipole couplings through the layers, further investigated by polarization measurements.[22] The SmC*(ferroelectric) phase presents a long pitch helical structure that strongly couples molecular dipoles through the layers. Conversely, as the ferrielectric phase forms, the helical pitch suddenly decreases denoting a weakening in the layer coupling.[1,22] Now, it is reasonable to think that the xenon atoms diffuse more easily through the loose layer arrangement of the SmC*(ferrielectric) phase with respect to the one of the SmC*(ferroelectric) phase; in terms of the free-volume model the SmC*(ferrielectric) phase presents higher volume fluctuations in respect to the SmC*(ferroelectric) one, facilitating the formation of cavities large enough for the xenon atoms to diffuse through and consequently: $\Delta E_{||(\text{ferroelectric})} > \Delta E_{||(\text{ferrielectric})}$.

The SmC*(antiferroelectric) phase is characterized again by a helical structure with a pitch length comparable with the SmC*(ferroelectric) phase but presents a tilt angle zigzag arrangement through the layers. That is, as the SmC*-(antiferroelectric) phase forms, a new order is established in an anticlinic arrangement of the phase director through the layers. Hence, the SmC*(antiferroelectric) phase structure hinders again the out-of-plane diffusion of xenon atoms due to the rigorous tilt angle alternation between the layers and $\Delta E_{||(\text{antiferroelectric})} > \Delta E_{||(\text{ferrielectric})}$.

This phenomenon has to be investigated in more details, possibly on similar systems, but it can be a sensitive probe to change in layer coupling and arrangement in SmC* sub-phases. The ferrielectric phase can hence be seen as a weak intermediate arrangement between the SmC* ferroelectric and antiferroelectric phases with opposite polar and tilt angle order.

Conclusions

The temperature-dependence of the ^{129}Xe shielding constant in the chiral 10B1M7 smectogen reveals clearly the isotropic−smectic A and smectic A−smectic C*(ferroelectric) phase transitions. On the contrary, only small changes in the shielding may be detected at the transitions within the C* phases, due to the subtle variations that happen in these sub-phases. It appeared that dissolved xenon shifts the phase transition temperatures by 3−4 K to low temperature as compared to the ones determined by optical methods for the pure compound. The application of a theoretical model to the experimental ^{129}Xe shielding data allows the determination of the isotropic shielding constant and the anisotropy of the shielding tensor. Furthermore, the analysis reveals that the xenon distribution differs from the uniform distribution; part of the xenon atoms is expelled from the dense core region to the less dense interlayer space during the formation of the smectic phase in the transition from the isotropic phase. This is in agreement with the earlier findings observed at the nematic−smectic A phase transitions.

For the first time, ^{129}Xe NMR spectroscopy is utilized in the derivation of the temperature-dependence of the tilt angle of the director in the smectic C* phases. The method is based on the assumptions that the liquid-crystal density and the three orientational order parameters do not change abruptly at the smectic A−smectic C* transition. The resulting tilt angle behavior is in fair agreement with the ones derived by other means.

Diffusion measurements of the dissolved xenon revealed a sharp change as the 10B1M7 LC assembles in the smectic A structure from the isotropic phase and a large anisotropy of the diffusion tensor, the ratio $D_\perp/D_{||}$ being much bigger than unity, in the SmA and SmC* phase. This can be explained by the fact that xenon atoms preferentially diffuse across the aliphatic regions ($D_\perp$) in the interlayer space than across the dense and more ordered aromatic cores ($D_{||}$). The diffusion activation energies, determined assuming an Arrhenius behavior in the 10B1M7 phases resulted in $E_{a||} > E_{a\perp}$, as can be expected from the anisotropy of the diffusion tensor, whereas the fact that $E_{a||}$(SmC*) > $E_{a||}$(SmA) can be a consequence of the appearance of the tilt angle. Finally, the relation $E_{a||(\text{ferroelectric})} \approx E_{a||(\text{antiferroelectric})} > E_{a||(\text{ferrielectric})}$ was found in the SmC* phases. This can be interpreted as a decrease in layer ordering in the intermediate SmC*(ferrielectric) phase passing from the synclinic ferroelectric and antiferroelectric to the anticlinic SmC*.

Acknowledgment. J.J. and J.S. are grateful to the Academy of Finland for financial support (Grant 43979). J.S. also thanks the Finnish Cultural Foundation for a grant. M.C. thanks the Università degli Studi di Pisa for the PhD scholarship and financial support.

References and Notes

(1) Muševič, I.; Blinc, R.; Žekš, B. *The Physics of Ferroelectric and Antiferroelectric Liquid Crystals*; World Scientific Publications: London, 2000.

(2) Takatoh, K.; Yamaguchi, H.; Hasegawa, R.; Saishu, T.; Fukushima, R. *Polym. Adv. Technol.* **2000**, *11*, 413.

(3) Jokisaari, J. *Prog. NMR Spectrosc*. **1994**, *26*, 1.
(4) Jokisaari, J. NMR of Noble Gases Dissolved in Liquids Crystals. In *NMR of ordered liquids*; Burnell, E. E., de Lange, C. A., Eds.; Kluwer: Dordrecht, 2003; pp 109−135.
(5) Bharatam, J.; Bowers, C. R. *J. Phys. Chem. B* **1999**, *103*, 2510.
(6) Diehl, P.; Jokisaari, J. *Liq. Cryst*. **1990**, *7*, 739.
(7) Lounila, J.; Münster, O.; Jokisaari, J.; Diehl, P. *J. Chem. Phys*. **1992**, *97*, 8977.
(8) Ruohonen, J.; Ylihautala, M.; Jokisaari, J. *Mol. Phys*. **2001**, *99*, 711.
(9) Catalano, D.; Cavazza, M.; Chiezzi, L.; Geppi, M.; Veracini, C. A. *Liq. Cryst*. **2000**, *27*, 621.
(10) Catalano, D.; Cifelli, M.; Geppi, M.; Veracini, C. A. *J. Phys. Chem. A* **2001**, *105*, 34.
(11) Veracini, C. A. Oral communication, ECLC, Jaca, Spain, April 2003.
(12) Stejskal, E. O.; Tanner, J. E. *J. Chem. Phys*. **1965**, *42*, 288.
(13) Norwood, T. J. *J. Magn. Reson. A* **1993**, *103*, 258.
(14) Ylihautala, M.; Lounila, J.; Jokisaari, J. *J. Chem. Phys*. **1999**, *110*, 6381.
(15) *Handbook of Liquid Crystals*; Demus, D., Goodby, J., Gray, G. W., Spiess, H.-W., Vill, V., Eds.; Wiley-VCH: Weinheim, Germany, 1998; Vol. 1, p 334.
(16) Haller, I. *Prog. Solid State Chem*. **1975**, *10*, 103.
(17) Buka, A.; de Jeu, W. H. *J. Phys*. *(Paris)* **1982**, *43*, 361.
(18) Meyer, R. B. *Mol. Cryst. Liq. Cryst*. **1977**, *40*, 33.
(19) Chandani, D. D. L.; Ouchi, Y.; Takezoe, H.; Fukuda, A.; Terashima, K. *Jpn. J. Appl. Phys*. **1990**, *28*, L1261.
(20) Wise, R. A.; Smith, D. H.; Doane, J. W. *Phys. Rev*. A **1973**, *7*, 1366.
(21) Chandrasekhar, S. *Liquid Crystals*, 2nd ed.; Cambridge University Press: New York, 1992.
(22) Goodby, J. W.; Patel, S.; Chin, E. *J. Mater. Chem*. **1992**, *2*, 197.
(23) Price, W. S.; Kuchel, P. W. *J. Magn. Reson*. **1991**, *94*, 133.
(24) Moseley, M. E. *J. Phys. Chem*. **1983**, *87*, 18.
(25) Moscicki, J. K.; Shin, Y. K.; Freed, J. *J. Chem. Phys*. **1993**, *99*, 634.
(26) Krüger, G. J. *Phys. Rep*. **1982,** *82*, 229.